Journal of Alloys and Compounds 896 (2022) 163063

Contents lists available at ScienceDirect

Journal of Alloys and Compounds

journal homepage: www.elsevier.com/locate/jalcom

Formic acid gas sensor based on coreless optical fiber coated by molybdenum disulfide nanosheet

Gaoliang Chen (陈高亮)[a], Jin Li (李晋)[a,b,c,*], Fanli Meng (孟凡利)[a]

[a] College of Information Science and Engineering, Northeastern University, Shenyang 110819, China
[b] State Key Laboratory of Applied Optics, Changchun Institute of Optics, Fine Mechanics and Physics, Chinese Academy of Sciences, Changchun 130033, China
[c] Hebei Key Laboratory of Micro-Nano Precision Optical Sensing and Measurement Technology, Qinhuangdao 066004, China

ARTICLE INFO

Article history:
Received 6 July 2021
Received in revised form 11 November 2021
Accepted 29 November 2021
Available online 1 December 2021

Keywords:
Formic acid gas
No-core fiber
Molybdenum disulfide nanosheets
Room temperature
Sensitivity

ABSTRACT

Molybdenum disulfide (MoS_2) nanosheets were prepared by the method of liquid phase ultrasonic separation. It is coated on the surface of single mode-no-core-single mode (SNS) fiber structure by drip coating method, which realizes the detection of formic acid gas under room temperature. The corresponding sensing performance has been discussed in the concentration range of 0–250 ppm and 0–1100 ppm, respectively. The good selectivity, repeatability and response/recovery characteristics have been experimentally demonstrated and used for exploring an effect method to greatly improve the sensitivity of the formic acid gas sensor. This passive optical fiber probe has the promising potential application in medical and industrial production process for determining the formic acid concentration at room temperature.

1. Introduction

Formic acid is a volatile organic compound and widely used in the pharmaceutical, tanning and other industries, acting as a kind of disinfectant, antiseptic and organic chemical raw material. Its pungent odor steam can corrode production equipment, damage the nervous system of human, and cause blindness for the long-term exposure [1]. It easily forms explosive mixtures with air. Therefore, the detection of formic acid gas in a relatively closed environment is extremely necessary.

With the development of gas sensing technology, the formic acid gas detection has also been concerned in the last few years. For example, in 2011, Yan et al. used electrochemical methods to plate a polyaniline film on the surface of the silver electrode to fabricate a quartz microbalance sensor for formic acid gas detection [2]. But its real-time performance is poor due to the slow migration rate of electrons. In 2016, Lu et al. prepared tungsten trioxide nanosheets by hydrothermal method and coated them on the alumina ceramic tubes with gold electrodes to detect formic acid gas [3], the corresponding working temperature is as high as 370 °C limited by the gas activity of materials. In 2018, Lin et al. developed a carbon nanotube formic acid gas sensor, in which the detection limit as low as 83 ppb was obtained by detecting changes in material conductivity [4]. However, the detection performance is affected by the response process and the poor recovery. In 2019, Liu et al. developed an impedance sensor for formic acid detection using a proton-conducting cobalt-organic framework [5], which has the strict requirements for the environmental humidity. In 2020, Kaewsiri et al. explored a formic acid gas sensor based on spinel Zn_2/SnO_3 nanoparticles [6]. Recently, Yuan et al. also proposed a semiconductor formic acid gas sensor using molybdenum disulfide (MoS_2) as a sensitive material [7]. For these electrochemistry mechanism sensors, the working temperature must be above 200 °C to promise the gas activity and the electrons transfer process is easily affected by the electromagnetic interference in complex environments. In addition to the room temperature working property compared to the electrochemistry gas sensors, the optical fiber gas sensor also has the characteristics of small size, light weight, and resistance to electromagnetic interference. Its sensitivity and selectivity performance can also be improved by the elaborating materials.

Nanomaterials often directly determines the sensing performance, playing an important role in semiconductor gas sensors. MoS_2 nanosheets have become a very valuable sensor material due to their superior semiconductor properties and high specific surface area [8]. Therefore, a great progress has been made on the research of MoS_2 nanomaterials in recent years. Various preparation

* Corresponding author at: College of Information Science and Engineering, Northeastern University, Shenyang 110819, China.
E-mail addresses: 1970567@stu.neu.edu.cn (G. Chen), lijin@ise.neu.edu.cn (J. Li), mengfanli@ise.neu.edu.cn (F. Meng).

https://doi.org/10.1016/j.jallcom.2021.163063
0925-8388/

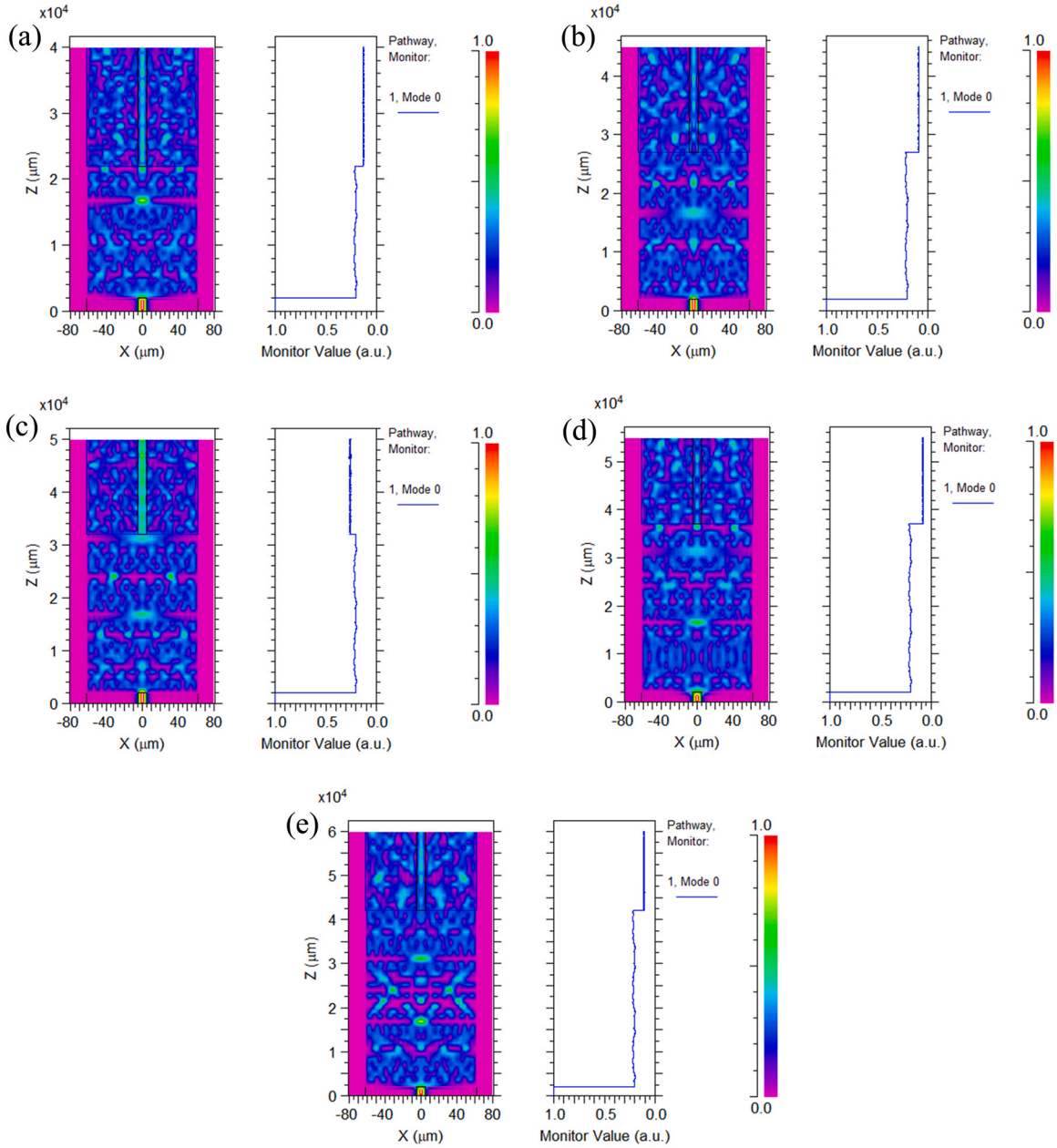

Fig. 1. (a)–(e) are the optical field distribution (left) and energy change (right) diagrams of SNS fiber structures containing 2 cm, 2.5 cm, 3 cm, 3.5 cm and 4 cm coreless fibers, respectively.

techniques have been developed, such as mechanical peeling [9], liquid phase ultrasonic separation [10] and chemical synthesis [11]. In this work, the liquid-phase ultrasonic separation technology was used to prepare MoS_2 nanosheets, due to its simple operation, low cost, and large-scale production. An optical fiber formic acid gas sensor based on the multi-mode interference of single mode-no core-single mode fiber (SNS) structure was introduced and adopted MoS_2 nanosheets as the sensitive film.

2. Experimental

2.1. Fiber structure

No core fiber is special in its structure with only a core and no cladding, named a cylindrical waveguide with uniform refractive index distribution. The multi-mode interference can be excited by different fiber structures, such as the SNS, single mode-multi modes-single mode (SMS), micro-nano fiber and other special fibers. The SMS structure itself is not sensitive to the outside world and requires the precise parameters control for the chemical corrosion [12] or mechanical peeling [13–16] process. The micro-nano fiber has poor mechanical strength and is easily broken. Other special fibers, such as photonic crystal fibers, are expensive. The SNS structure has the advantages of simple operation, high stability and low cost [17]. These features will provide great convenience for subsequent coating operations. The length change of single mode fiber and no core fiber will not affect the sensitivity characteristics of the SNS structure [18], but the position of the interference peak will be affected by the length of the no less fiber. In order to further determine the specific parameters of the optical fiber structure, the Rsoft simulation software is used to simulate the SNS structure. As shown in Fig. 1(a)–(e) are the optical field distribution and energy change diagrams of the fiber structure, which respectively contain 2 cm, 2.5 cm, 3 cm, 3.5 cm, 4 cm coreless fibers.

It can be found from the figure that the optical self-reflection effect point of the coreless waveband is located near 3 cm. Therefore, when the length of the coreless fiber is about 3 cm, the optical transmission effect of the fiber structure is the best, and the optical coupling efficiency is the highest. This is conducive to the transmission of light energy, reducing transmission loss and light wave burrs. And the wavelength of the light source in the simulation process is 1550 nm, which is in the middle of the light excited by the actual light source (the wavelength range is generally 1520–1570 nm). The light extreme point is located just around 3 cm, so it is more conducive to the appearance of interference spectra. Therefore, a cut of 3 cm length no core fiber (CL1010-A of YOFC) was chosen and spliced between two sections of ordinary single-mode fiber (G652D of YOFC) to carry out the SNS structure. In this way, the sensitivity is ensured and the subsequent coating process is simplified. The specific experimental operation is as follows: 1. Preparing two sections of single mode fibers and one cut of no core fiber with flat and clean surface using the fiber cleaver; 2. Splicing the no core fiber with one single mode fiber using the automatic fusion splicing program of the fiber fusion splicer; 3. Cutting the desire length of no core fiber and splicing its other end with another single-mode fiber. The no core fiber part acts as the sensing area to be coated. Then, the fusion spliced optical fiber sensing area was wiped clean, dried, and fixed on a clean glass slide for later use.

2.2. Preparation and characterization of sensitive materials

The MoS_2 nanosheets were prepared by ultrasonic liquid phase separation [3,7,19]. The chemical reagents used in the experiment were all analytical pure. Usually, 225 ml of absolute ethanol and 275 ml of pure water were thoroughly mixed to form ~500 ml of ethanol solution with a volume fraction of 45%, which will be later used to disperse the MoS_2. Then the purchased MoS_2 raw material was put into the muffle furnace, heated from room temperature to 270 °C with a temperature increase rate of ~ 2 °C per minute, and calcinated at 270 °C for 3 h. Then, the cool-treated MoS_2 into was dispersed in a 45% ethanol solution, in which an appropriate amount of sodium hydroxide was added before the ultrasonic process to improve the peeling effect [19]. The MoS_2 dispersion was put into an ultrasonic cleaning machine with a power of 600 W for the ultrasonic treatment of 12 h. The ultrasonic dispersant was centrifuged at 4000 r/min for 6 min to obtain the supernatant solution, which was later centrifugal separated at a speed of 8000 r/min to get the precipitate. It was added into an appropriate amount of 45% ethanol to dissolve and disperse. The previous centrifugation operation was repeated again to prepare the MoS_2 nanosheet dispersion solution. During the centrifugation process, the solutions must be handled gently, and moved as quickly as possible. Otherwise, the centrifugal effect will be affected, and the content ratio of the MoS_2 thin-layer nanosheets will be reduced. It should be noted that a hard container should be used during the ultrasonic treatment to benefit the ultrasonic peeling efficiency. The prepared MoS_2 nanosheet dispersion liquid was dropped on a clean silicon wafer, which was evaporated to dryness on a heating platform at a constant temperature and characterized by SEM.

2.3. Test system

The schematic diagram of the gas testing system is shown in Fig. 2. The light source is the ASE broadband light source (KG-ASE-CL-D-13-FC/APC) with the working wavelength of 1528–1603 nm. The air chamber is spliced by acrylic plates and has a volume of 2 L, on whose left and right sides the optical fiber flange interfaces were equipped to connect the optical fibers. The smaller vent hole in the upper left corner is used to inject in gas, while the two larger vent holes on the front and back are used to discharge the test gas. The two rotatable channels on top facilitate the placement of fiber probe. The spectrometer is the Yokogawa Spectral Scanner (AQ6370D) with the resolution of 0.02 nm, which is used to display and record spectra. It can collect spectral data with 0.004 nm intervals.

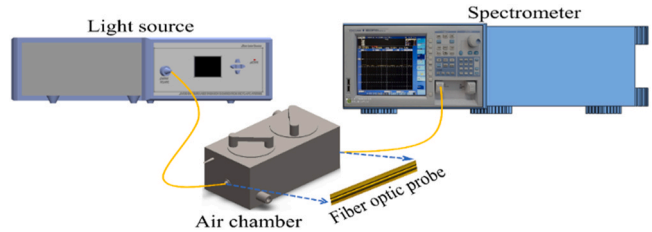

Fig. 2. Schematic diagram of optical fiber gas sensor test system.

2.4. Fiber elaboration

During the drip coating process, the optical fiber structure maintains being connected in the test system, where the interference spectrum was real-time observed in the spectrometer to judge the coating quality. First, the prepared optical fiber structure was placed on a heating platform. The interference spectrum was recorded as the background in the spectrometer. A pipette was used to suck up an appropriate amount of the prepared MoS_2 nanosheet dispersion solution, which were dropped slowly and evenly onto the sensing area. The solution will be completely evaporated to dryness film at a constant temperature of ~ 100 °C. This drip coating process has been repeated several times until a significant red shift (the interference peak moves to a longer wavelength) can be observed in the interference spectrum. Meanwhile, the significant transmission loss was caused by the light leakage at the interface of optical fiber and elaborating MoS_2 film. A more obvious difference will result in a higher sensitivity, because more MoS_2 nanosheets were attached onto the fiber surface in this situation. However, the coating dose must be carefully controlled since too much/thick MoS_2 nanosheets will seriously reduce the response and recovery rate. In actual operation, the amount of movement of the interference peak can be observed to determine and control how much MoS_2 nanosheets are attached. Therefore, during the experiment, the whole fiber structure is connecting in the measurement system to real-time monitor the interference spectrum by the spectrometer to promise the reproducibility of the proposed MoS_2 nanosheet coating quality, including the number of coatings layer and the consistent the fiber structures.

3. Results and discussion

3.1. MoS_2 nanosheets and coating effect

Fig. 3(a, b) refer to the SEM images of MoS_2 raw material and nanosheets respectively. Compared with the thick slabs of the raw materials, the obtained MoS_2 nanosheets distribute uniformly in the shape of small flakes.

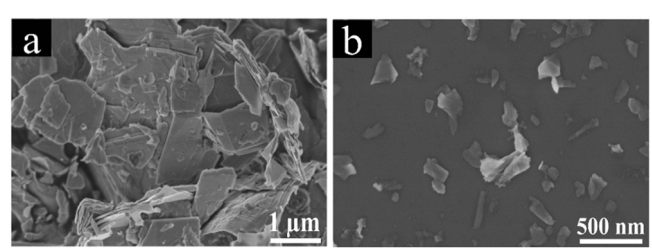

Fig. 3. SEM images of MoS_2 (a) before and (b) after ultrasonic separation.

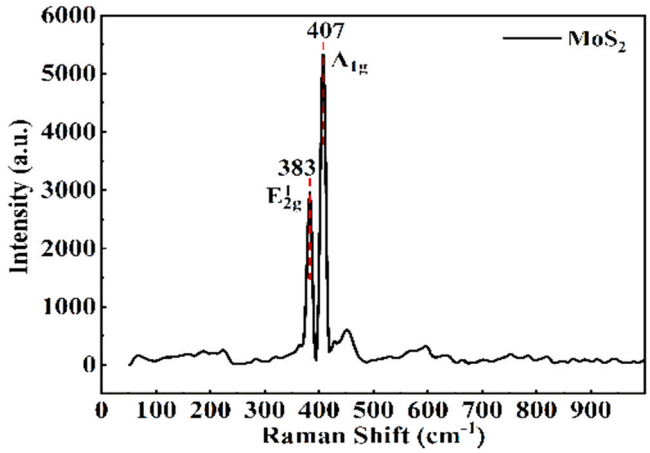

Fig. 4. Raman spectrum of MoS_2 nanosheet.

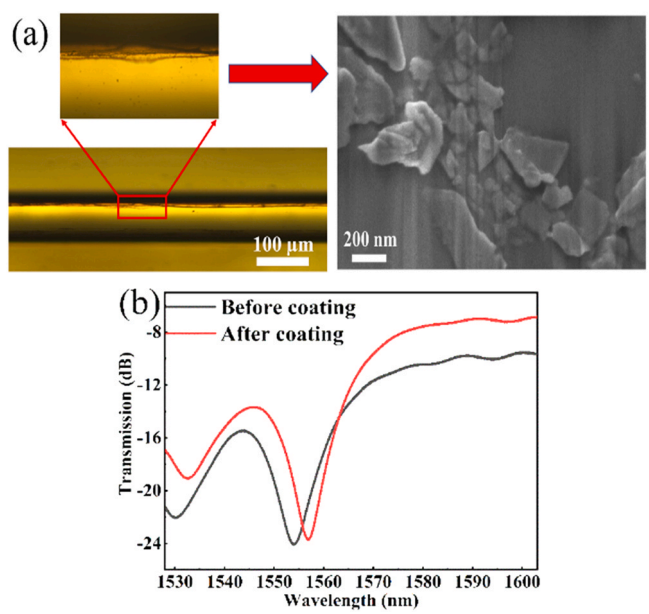

Fig. 5. (a) Microscope and SEM images of fiber structure coated with MoS_2 nanosheets. (b) Spectrum comparison for fiber structure before and after coating.

Fig. 4 shows the Raman characterization results of MoS_2 nanosheets. Two Raman characteristic peaks at 383 cm^{-1} and 407 cm^{-1} are found, corresponding respectively to Raman vibration modes E^1_{2g} and A_{1g} of MoS_2 nanosheets [20] and indicating the oxidation generation. In addition, no other Raman vibration modes can be found here, verifying the purity of the MoS_2 nanosheets peeled off during the ultrasonic stripping process. MoS_2 nanosheets with different layers correspond to the different Raman characteristic peaks [21]. As the thickness of the MoS_2 nanosheet decreases, the wavenumber difference between its E^1_{2g} and A_{1g} Raman vibration modes also gradually decreases. The wavenumber difference of the Raman vibration mode of the prepared MoS_2 nanosheets is 24 cm^{-1}, which is consistent with the 4-layer MoS_2 nanosheets [22].

Fig. 5(a) shows the microscope picture and SEM image of the sensing area on the elaborated fiber, where the plated material is tightly attached on the outer surface. Because of the hydrophobicity of MoS_2, the nano-materials become aggregated. In addition to the non-uniformity, the adhesion effect and mechanical stability of the coating film has been significantly improved in this way. Fig. 5(b) compares the different interference spectra of the SNS fiber structure before and after coating. After the coated process, a significant red-shift was recorded in the interference spectrum, depending on the decrease of the equivalent refractive index difference between no core fiber and coating film, caused by the attached MoS_2 nanosheets [23].

3.2. Gas sensing properties and sensing mechanism

3.2.1. Small concentration range

Under room temperature conditions (25 ± 1 °C), the gradient test was performed on the fiber probe coated with MoS_2 nanosheets in the gas concentration range of 0–250 ppm with an interval of 50 ppm. The formic acid gas comes from the analytically pure formic acid liquid. In the reagent bottle, formic acid gas will naturally volatilize and reach a saturated state up the liquid surface. It will be drawn by a syringe and injected directly into the intake chamber. This method has been introduced and reported in several works earlier [20,21]. During the exhaust process, the natural emptying method was used to restore the air chamber with the natural free flow air same to the outer environment, and the sensor recovery process is completed. During the experiment, the humidity of the air in the air chamber is ~42% RH, and the purity of the dried formic acid gas is 100%. As shown in Fig. 6(a), as the concentration of formic acid gas increases, the interference spectrum gradually shifts to the long wavelength direction. The linear fitting was performed on the concentration of formic acid gas and the wavelength shift amount of the interference valley, as shown in Fig. 6(b). The detection limit was determined to be 50 ppm depending on the resolution of 20 pm for the spectrometer used in this work. In the concentration range of 0–250 ppm, there is a certain linear relationship (linearity: 0.89286) and a sensitivity of 0.114 pm/ppm.

3.2.2. Large concentration range

To expand the working range of the proposed formic acid gas probe, different gas concentration (0–1100 ppm) was injected into

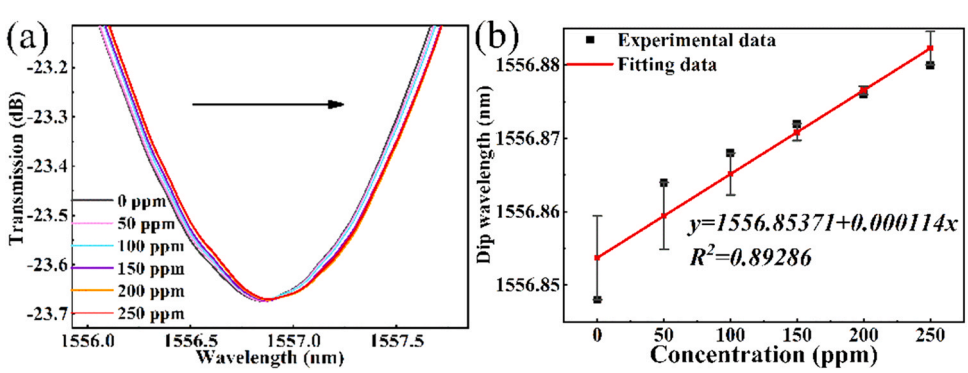

Fig. 6. (a) Sensor spectrum and (b) relationship of wavelength shift vs gas concentration for formic acid gas with a small range of 0–250 ppm.

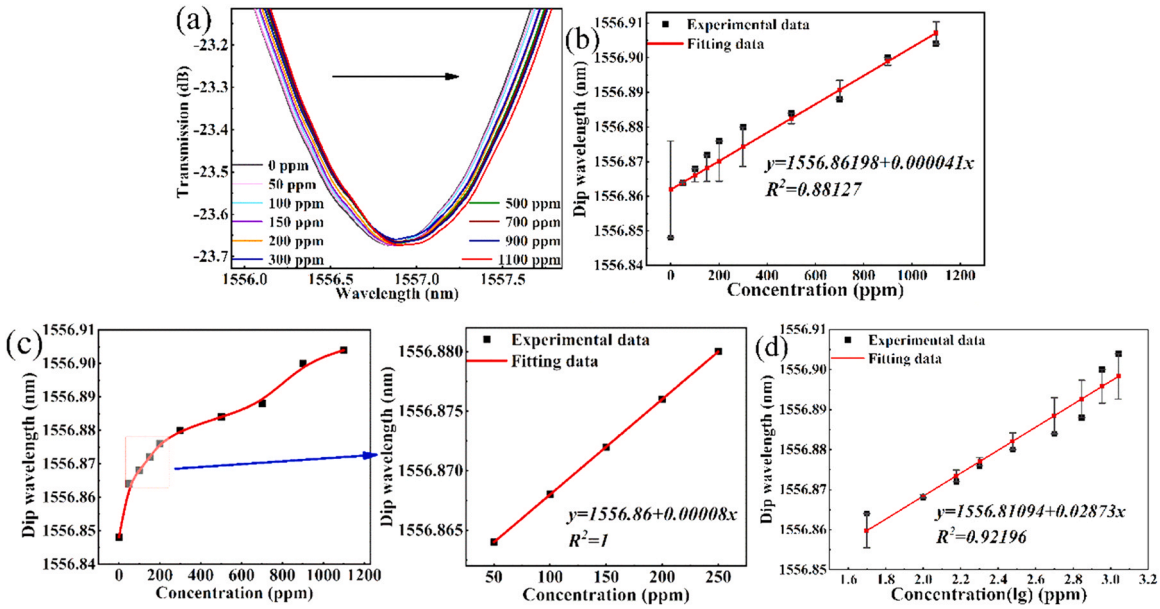

Fig. 7. (a) Sensing spectrum under a wide range (0–1100 ppm) of formic acid gas concentration. (b) Linear and (c) non-linear fitting between wavelength shift and gas concentration. (c) Enlarge section and (d) simple logarithmic calculation of gas sensing characteristics curve in the concentration range of 50–250 ppm.

the gas chamber respectively. As shown in Fig. 7(a), as the concentration continues increase, the interference valley produces a larger red shift. The corresponding wavelength locations as a function of gas concentration has been illustrated in Fig. 7(b). Compared with the previous results of small concentration range, the overall linearity became worse in the 0–1100 ppm concentration range. It is concerned that sub-interval indicates a good linearity in the concentration range of 50–250 ppm, as shown in Fig. 7(c). To completely calibrate the sensing performance in the whole concentration range, a simple logarithmic operation was carried, the corresponding result is shown in Fig. 7(d). Its linearity is significantly improved to 0.92196, and the sensitivity can be expressed as 28.73 pm/ppm(log). In addition, similar to most gas sensors, the response curve will gradually tend to be saturated with the gradual increase of the gas concentration, which will inevitably lead to a sensitivity decrease in the high-concentration range. During the actual calibration process, an appropriate calibration method and working range should be optimized according to the actual needs and sensing performance characteristics.

3.2.3. Gas sensing mechanism

Since the MoS_2 nanosheets obtained by liquid phase separation are N-type semiconductors, in which the electrons play as the majority carriers [24]. As shown in Fig. 8(a), when formic acid gas molecules are attached on the MoS_2 nanosheets, one part of electrons will be transferred from MoS_2 nanosheets to formic acid gas molecules, leading to an increase in the dielectric constant (refractive index) of the MoS_2 nanosheet material [8,9]. The effective refractive index difference near the optical fiber sensing area will result in the red-shift in the interference spectrum. Fig. 8(b) shows the simulation results of the influence of the refractive index changes of the external environment (equivalent to MoS_2 nanosheets) on the transmission spectrum, where the refractive index of a single-layer MoS_2 nanosheet is similar to that of pure water. The interference spectrum gradually redshifts with the increasing of the external refractive index, which is consistent with the experimental results.

3.3. Selectivity, repeatability, response, and recovery characteristics

Fig. 9. shows the selectivity test results of the proposed gas probe under the same concentration of 100 ppm for different gas sample, such as aniline, chlorobenzene, butyl acetate, formaldehyde, methyl ethyl ketone, xylene, styrene, benzene, n-propanol, acetaldehyde, toluene, isopropanol, acetone, methanol and ethanol. Only formic acid gas has an obvious response at room temperature, indicating an excellent selectivity, which is largely due to the function of the carboxyl group of the formic acid molecule.

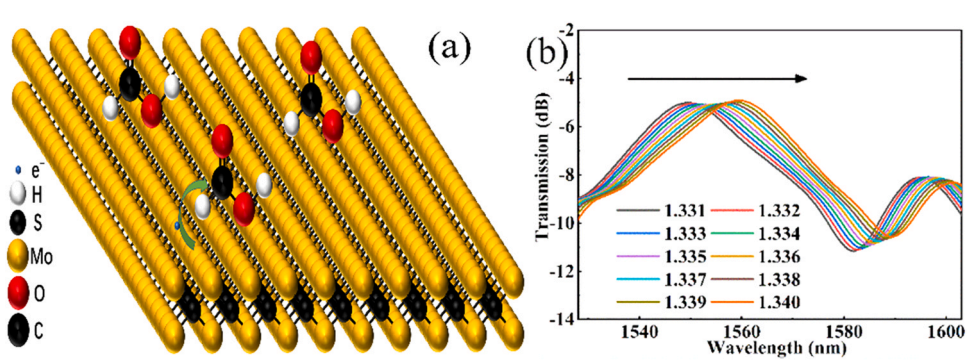

Fig. 8. (a) Response mechanism of MoS_2 nanosheets to formic acid gas. (b) Influence from refractive index change of external environment (MoS_2 nanosheets) on transmission spectrum of optical fiber structure.

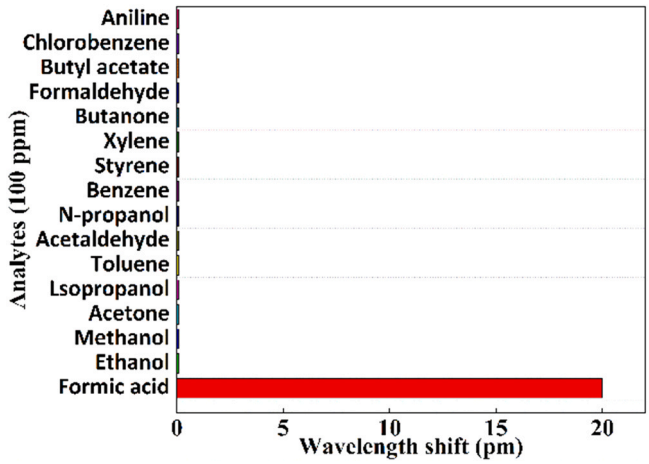

Fig. 9. Selectivity comparison of sensor in various gases with 100 ppm.

Under the same conditions, 100 ppm of formic acid gas was repeatedly injected into the gas chamber for several times and then discharged to study the response and recovery performance of the gas fiber probe. As shown in Fig. 10(a), the overlapped response and the recovery spectra for 5 consecutive times reveal a good repeatability. Fig. 10(b) and (c) indicate the response and recovery speed, respectively. As 100 ppm formic acid gas being introduced into the gas chamber, the sensor responds quickly within ~ 150 s. Then the gas chamber was opened and the formic acid gas freely diffused out, the transmission spectrum was restored after ~ 300 s. Compared with the tens of minutes [14] or even hundreds of minutes [13,15,16] for the same type of cladding improved fiber gas sensor, the response and recovery time have been greatly reduced.

The performance of the proposed sensor is compared with the formic acid gas sensors recently developed (Table 1). It can be found that the traditional electrochemical formic acid gas sensor has a higher working temperature [3,6,7], higher detection concentration [1,2], and the extremely demanding for humidity environment [5]. In addition, the electromagnetic signals cannot meet the standards of intrinsically safe instruments.

Table 1
Sensing performance comparison of formic acid gas sensors recently developed.

Ref.	Temperature (°C)	Concentration	t_{res}/t_{rec} (s)	LOD
[1]	25	7.3–100%	52/-	7.3%
[2]	24 ± 1	1,5,10,20 × 10^6 ppm	~ 3600/-	10^6 ppm
[3]	370	10–500 ppm	–	10 ppm
[5]	25	35/70–2100 ppm	–	35 ppm
[6]	350	50–1000 ppm	7.5_{least}/ ~ 3000	50 ppm
[7]	270	10–100 ppm	11/17	10 ppm
This work	25	50–250 ppm	150/300	50 ppm

4. Optimization of gas sensing properties

To further improve the sensing performance, the formic acid sensing performance of the proposed fiber sensor was studied being immersed in the ammonia atmosphere with a certain concentration. Under the same premise conditions, 50 ppm of ammonia gas was injected into the gas chamber in advance. After the spectrum becoming stable, its response for 0–400 ppm of formic acid gas was sequentially measured. As shown in Fig. 11(a), more obvious redshift has been observed. The sensing characteristic curve was linearly fitted in Fig. 11(b), compared with the results in Section 3.2.1 under the similar situation, the working range has been expanded to 400 ppm with a greatly improved linearity of 0.95142. More importantly, its sensitivity has increased to 1.13 pm/ppm, which is ~ 10 times higher than the previous value of 0.114 pm/ppm. This improvement can be contributed to the hydration reaction between ammonia (alkaline gas) and formic acid (acid gas), as well as the hydrophobic nature of the MoS_2 nanosheets. During the exhaust process, we saw a puff of white smoke wafting out of the gas

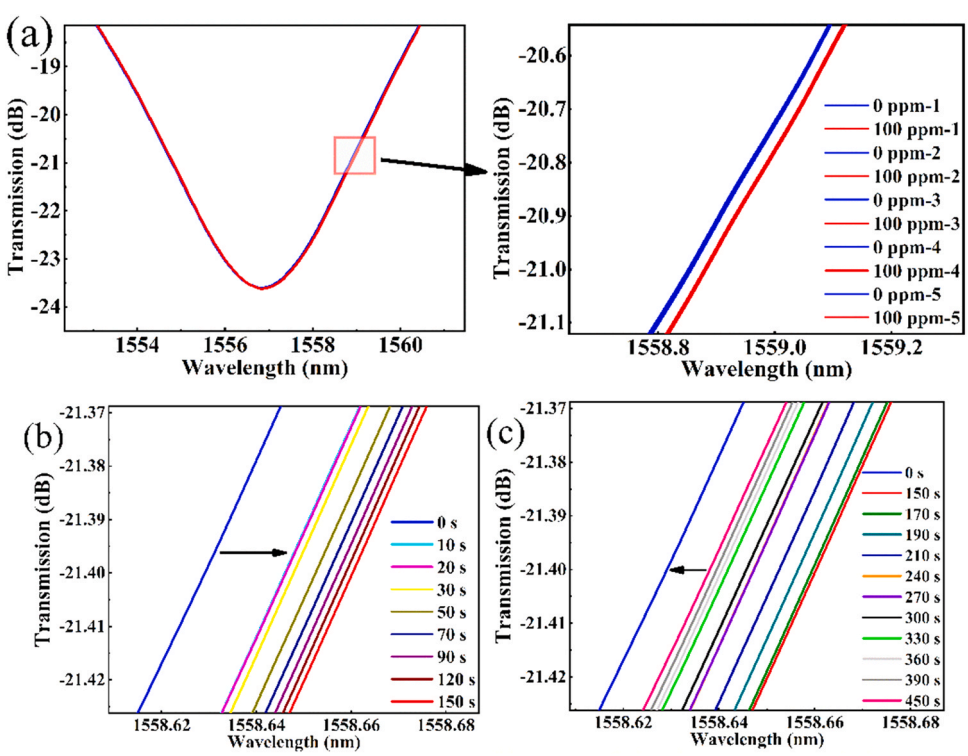

Fig. 10. (a) Repeatability, (b) response and (c) recovery characteristics of the sensor to 100 ppm formic acid gas.

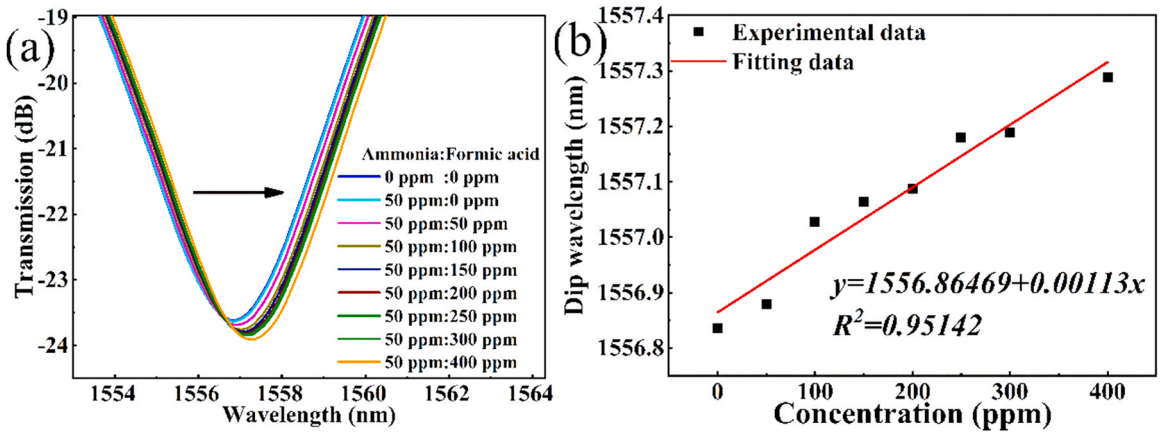

Fig. 11. (a) Response spectrum and (b) sensing characteristic curve of formic acid sensor in a 50 ppm of ammonia atmosphere.

chamber, presumably it was ammonium formate. In addition, we have made sure that there are not any new materials polluted the fiber surface by monitoring and comparing its interference spectrum before and after the experiment. Since the special wavelength of the dip in the interference is sensitive to the surrounding refractive index of the optical fiber. In our experiment, the special wavelength moved back to its original position, revealing that the fiber surface is clean as its prior status. We also observed its surface under a microscope, which is clean and transparent. Maybe there will be little ammonium formate fallen on the surface, but the impact can be ignored. Furthermore, the adsorption and desorption speed of water molecules on the surface of MoS_2 is very quickly [10]. Therefore, the response of the sensor to formic acid gas is effectively amplified and its sensitivity is significantly improved without any other negative impact. At the beginning, the MoS_2 nanosheets was wrapped by the ammonia molecules. For the low concentration of formic acid gas, the water molecules produced by the interaction of the two gases and affects the spectrum shift. As the concentration increases, the formic acid molecules further invade the adsorption sites on the surface of MoS_2 nanosheets and contributed to the adsorption effect of water molecules, finally resulting in higher sensitivity for formic acid gas in a larger measuring range. In addition, in the actual operation process, the detection limit, measurement range and sensitivity of the sensor can be balanced and adjusted by controlling the concentration of the ammonia atmosphere. In our experiment, a closed container with a known volume was used as a fixed test gas chamber, and a certain concentration of ammonia gas was injected into it to supply a test environment. Indeed, although the sensitivity can be significantly improved, the special working environment must rely on the cumbersome setup. There is still a lot of room for improvement for the actual application.

5. Humidity sensing performance and impact on gas sensing properties

In order to develop a gas sensor that works at room temperature, its humidity-sensitive characteristics and the influence of humidity changes on its gas-sensing characteristics must be clear.

5.1. Humidity sensitivity characteristics

At room temperature, the relative humidity (RH) in the air chamber is strictly controlled and regulated in the range of 20% RH to 75% RH. The response spectra are shown in Fig. 12(a). With the increase of humidity in the air chamber, the spectrum red-shifts gradually, which is caused by the hydrophobicity of the MoS_2 material itself. The curve of the spectral shift value as a function of RH is shown in Fig. 12(b). It can be clearly found that the sensor having the little wavelength shift, which indicating it is not sensitive to humidity during the low humidity section (20–50% RH); while a high sensitivity was demonstrated in the high-humidity section (50–75% RH). Therefore, the probe can be used as a humidity sensing probe in a high humidity environment. However, as a gas sensor, the environmental humidity must be strictly controlled at a low level. In the actual application process, the environmental humidity is generally stable and not easy to change. For environments with obvious humidity changes, the humidity sensor can be connected in series to perform real-time humidity compensation. During the information demodulation process, the humidity interference can be eliminated by analyzing the two-dimensional correlation matrix containing the humidity and gas difference and their corresponding wavelength shift values.

5.2. Influence of RH on gas sensing performance

In order to further explore the influence of different RH on the gas sensing characteristics of the sensor, under the premise of relatively constant temperature of 25 ± 1 °C, the gas sensing characteristics for formic acid gas with the concentration of 0–400 ppm have been tested when the RH were 28% RH, 38% RH, 48% RH, 58% RH and 68% RH, respectively, with the corresponding results in Fig. 13. Under different humidity conditions, the sensor has a significantly different degree of response to formic acid gas.

The gas sensing curves in Fig. 13 illustrate that when the environmental RH maintains at 58% RH and 68% RH, the sensor's response to formic acid gas is significantly higher comparing to other RH values, having the maximum gas sensitivity at 68% RH. When RHs are 38% RH and 48% RH, especially for 38% RH, the gas sensitivity becomes worst, corresponding to the RH sensitivity of the fiber probe in Fig. 12(b), that is, during the humidity range with a higher RH sensitivity, the highest sensitivity for formic acid gas can also be obtained. It also further confirms that when formic acid gas is adsorbed on the surface of MoS_2 nanosheets, a certain amount of water molecules will be generated under the catalytic action of MoS_2 nanosheets. During the experiment, both the temperature and humidity in the air chamber have been strictly controlled and measured in real time. In addition, during the dynamic test, the humidity and temperature in the air chamber were timely monitored and strictly controlled, whose interference can be ignored during the whole experiment. Furthermore, the ventilation, response and acquisition time of each test are almost the same. The wavelength shift values were obtained in the relative difference way by comparing the characteristic wavelength position before and after the gas concentration change. The time for each step is too

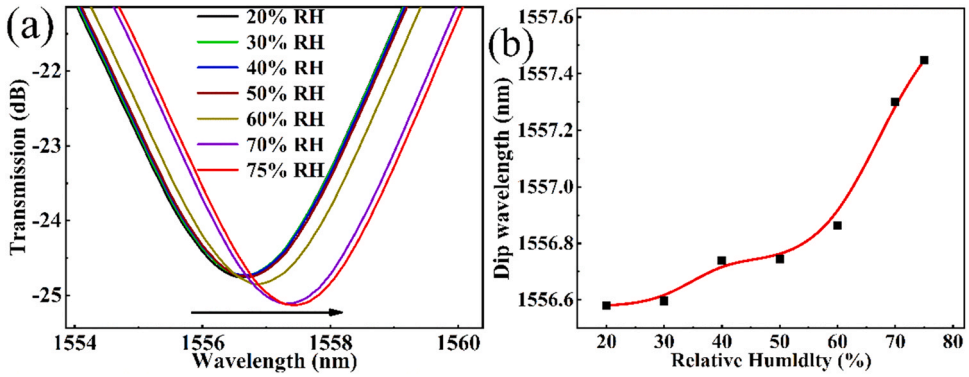

Fig. 12. (a) Spectra change under different relative humidity; (b) Relationship curve between wavelength shift and relative humidity during 20–75% RH.

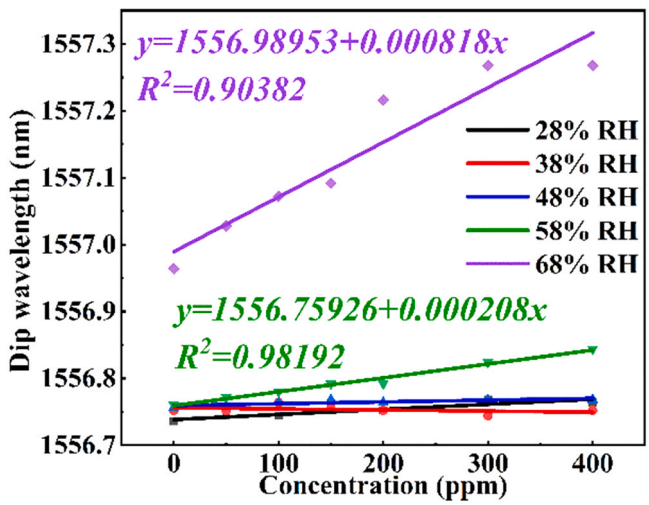

Fig. 13. Gas sensing curves under different RH of 28% RH, 38% RH, 48% RH, 58% RH, and 68% RH.

short, during when the impact from the environmental humidity and temperature can be naturally eliminated.

6. Conclusion

In this paper, the MoS_2 nanosheets coated SNS optical fiber probe has been experimentally demonstrated for detecting formic acid gas at room temperature. It paves a new way to determine formic acid gas in the long-distance at room temperature, overcoming the limitation of electrochemical sensors, such as the potential risks and threats from the complex electromagnetic and other complex environment. As far as we know, this is the first time to measure the concentration of formic acid gas using an optical fiber probe. An effective method has also been suggested to greatly improve the sensitivity. In the near future, a higher performance formic acid gas optical fiber sensor will be developed by optimizing the optical fiber structure, sensitive film or coating method.

CRediT authorship contribution statement

Gaoliang Chen: Data curation, Formal analysis, Investigation, Methodology, Writing – original draft. **Jin Li:** Funding acquisition, Supervision, Writing – review & editing. **Fanli Meng:** Funding acquisition, Project administration.

Declaration of Competing Interest

The authors declare that they have no known competing financial interests or personal relationships that could have appeared to influence the work reported in this paper.

Acknowledgement

This work was supported by the National Key R&D Program of China (2019YFB2006001), Fundamental Research Funds for Central Universities (N2004007), and Hebei Natural Science Foundation (F2020501040).

References

[1] S. Moonrinta, B. Kwon, I. In, S. Kladsomboon, W. Sajomsang, P. Paoprasert, Highly biocompatible yogurt-derived carbon dots as multipurpose sensors for detection of formic acid vapor and metal ions, Opt. Mater. 81 (2018) 93–101.
[2] Y. Yan, D.D. Lu, H. Zhou, H.P. Hou, T. Zhang, L.M. Wu, L.K. Cai, Polyaniline-modified quartz crystal microbalance sensor for detection of formic acid gas, Water Air Soil Pollut. 223 (2012) 1275–1280.
[3] N. Lu, X. Gao, C. Yang, F. Xiao, J. Wang, X. Su, Enhanced formic acid gas-sensing property of WO3 nanorod bundles via hydrothermal method, Sens. Actuators B-Chem. 223 (2016) 743–749.
[4] S.B. Lin, T.M. Swager, Carbon nanotube formic acid sensors using a nickel bis (ortho-diiminosemiquinonate) selector, Acs Sensors 3 (2018) 569–573.
[5] R.L. Liu, Z.Q. Shi, X.Y. Wang, Z.F. Li, G. Li, Two highly stable proton conductive cobalt(II)-organic frameworks as impedance sensors for formic acid, Chem. - A Eur. J. 25 (2019) 14108–14116.
[6] D. Kaewsiri, K. Inyawilert, A. Wisitsoraat, A. Tuantranont, S. Phanichphant, C. Liewhiran, Single-nozzle flame synthesis of spinel Zn_2SnO_4 nanoparticles for selective detection of formic acid, IEEE Sens. J. 20 (2020) 6256–6262.
[7] Z. Yuan, C. Yang, H. Gao, W. Qin, F. Meng, High response formic acid gas sensor based on MoS2 nanosheets, IEEE Trans. Nanotechnol. 20 (2021) 177–184 1-1.
[8] E. Akbari, K. Jahanbin, A. Afroozeh, P. Yupapin, Z. Buntat, Brief review of monolayer molybdenum disulfide application in gas sensor, Phys. B: Condens. Matter 545 (2018) 510–518.
[9] F.K. Perkins, A.L. Friedman, E. Cobas, P.M. Campbell, G.G. Jernigan, B.T. Jonker, Chemical vapor sensing with monolayer MoS2, Nano Lett. 13 (2013) 668–673.
[10] S.-L. Zhang, H.-H. Choi, H.-Y. Yue, W.-C. Yang, Controlled exfoliation of molybdenum disulfide for developing thin film humidity sensor, Curr. Appl. Phys. 14 (2014) 264–268.
[11] X. Liu, L. Jiang, X. Jiang, X. Tian, Y. Huang, P. Hou, S. Zhang, X. Xu, Design of superior ethanol gas sensor based on indium oxide/molybdenum disulfide nanocomposite via hydrothermal route, Appl. Surf. Sci. 447 (2018) 49–56.
[12] Y. Jianming, M.A. El-Sherif, Fiber-optic chemical sensor using polyaniline as modified cladding material, IEEE Sens. J. 3 (2003) 5–12.
[13] B. Renganathan, D. Sastikumar, R. Srinivasan, A.R. Ganesan, Nanocrystalline samarium oxide coated fiber optic gas sensor, Mater. Sci. Eng.: B 186 (2014) 122–127.
[14] M. Subramanian, V.V. Dhayabaran, D. Sastikumar, M. Shanmugavadivel, Development of room temperature fiber optic gas sensor using clad modified Zn3 (VO4)2, J. Alloy. Compd. 750 (2018) 153–163.
[15] B. Renganathan, D. Sastikumar, G. Gobi, N. Rajeswari Yogamalar, A. Chandra Bose, Nanocrystalline ZnO coated fiber optic sensor for ammonia gas detection, Opt. Laser Technol. 43 (2011) 1398–1404.
[16] B. Renganathan, A.R. Ganesan, Fiber optic gas sensor with nanocrystalline ZnO, Opt. Fiber Technol. 20 (2014) 48–52.

[17] W. Yan, Q. Han, Y. Chen, H. Song, X. Tang, T. Liu, Fiber-loop ring-down interrogated refractive index sensor based on an SNS fiber structure, Sens. Actuators B: Chem. 255 (2018) 2018–2022.
[18] Y. Li, Z. Liu, S. Jian, Multimode interference refractive index sensor based on coreless fiber, Photon. Sens. 4 (2013) 21–27.
[19] G.S. Bang, K.W. Nam, J.Y. Kim, J. Shin, J.W. Choi, S.Y. Choi, Effective liquid-phase exfoliation and sodium ion battery application of MoS2 nanosheets, ACS Appl. Mater. Interfaces 6 (2014) 7084–7089.
[20] T. Guo, L. Wang, S. Sun, Y. Wang, X. Chen, K. Zhang, D. Zhang, Z. Xue, X. Zhou, Layered MoS2@graphene functionalized with nitrogen-doped graphene quantum dots as an enhanced electrochemical hydrogen evolution catalyst, Chin. Chem. Lett. 30 (2019) 1253–1260.
[21] C. Lee, H. Yan, L.E. Brus, T.F. Heinz, J. Hone, S. Ryu, Anomalous lattice vibrations of single-and few-layer MoS2, ACS Nano 4 (2010) 2695–2700.
[22] H. Samassekou, A. Alkabsh, M. Wasala, M. Eaton, A. Walber, A. Walker, O. Pitkänen, K. Kordas, S. Talapatra, T. Jayasekera, Viable route towards large-area 2D MoS2 using magnetron sputtering, 2D Mater. 4 (2017) 021002.
[23] Y. Bai, Y. Miao, H. Zhang, J. Yao, Simultaneous measurement of relative humidity and temperature using a microfiber coupler coated with molybdenum disulfide nanosheets, Opt. Mater. Express 9 (2019) 2846.
[24] Z. Wang, B. Mi, Environmental applications of 2D molybdenum disulfide (MoS2) nanosheets, Environ. Sci. Technol. 51 (2017) 8229–8244.